Chronic shallow seawater circulation driven by subsurface gas dynamics, at the Southern Hydrate Ridge seep system, Cascadia

Lauren Kowalski[1]

Advisor: Evan Solomon[1]
[1]University of Washington, School of Oceanography, Box 357940, Seattle, Washington, 98195-7940
(401) 578-6794
lak32@uw.edu
May 31, 2016

1. ABSTRACT

Cold seeps, like Southern Hydrate Ridge (SHR) on the Cascadia margin, are ubiquitous features along continental margins where fluids discharge from the seafloor into the water column. Previous short-term fluid flow studies at SHR and other seep systems have observed upward flow of altered fluids concentrated in regions of bacterial mats and downward flow of seawater-like fluids in regions of vesicomyid clams. To investigate longer-term variability in magnitude and direction of fluid flow at SHR, three continuous-measurement flowmeter/chemical samplers (Mosquitos) were deployed in bacterial mats to measure fluid flow rates and solute fluxes. This two-year continuous record of fluid flow shows that the flow rate at SHR is temporally and spatially variable, however there is an annual trend of ~24-67 cm/yr of downward fluid flow in regions of bacterial mats. This net downward transport of seawater circulation is more constant than previously recognized and the results indicate that shallow seawater circulation is the key in reconciling the discrepancy between bottom up and top down measurements of fluid flow at seep sites. Mechanisms driving this shallow seawater circulation are explored in addition to the connection between fluid flow and the ecology of associated benthic communities.

2. INTRODUCTION

Continental margin cold seeps are important regions for the exchange of fluids, solutes, gases, and isotope ratios between the lithosphere and the hydrosphere. Cold seeps are areas of concentrated fluid flow that are globally ubiquitous along continental margins, and are also found in other tectonic settings. These seeps are different from hydrothermal vents as they emit fluids at or just above ambient temperature from sediments into the water column rather than high temperature fluids from oceanic basalt. At subduction zones, these seeps are expressed at fault zones and in regions where permeable sediments such as sand horizons outcrop at the seafloor

(Figure 1). The chemical composition of the fluid expelled at seep sites is often distinct from the surrounding seawater due to sub-seafloor fluid rock reactions within the subduction zone (Kastner et al., 2014). This altered fluid is important in driving the numerous biogeochemical processes that allow diverse biological communities to thrive at these seep sites (Boetius & Suess 2004).

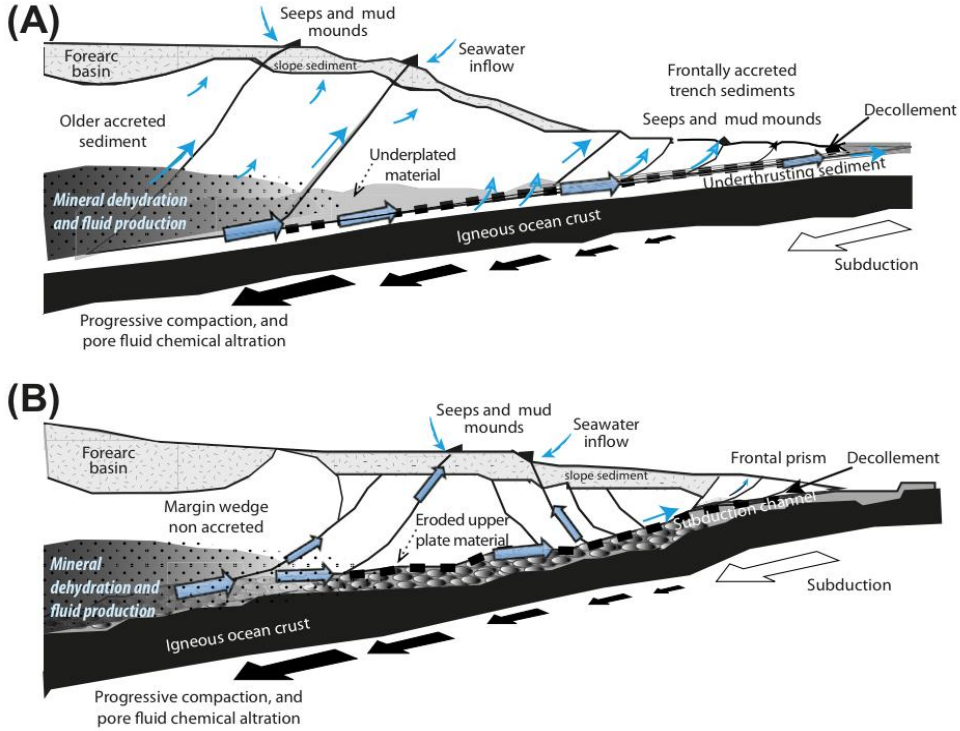

Figure 1. Diagrams representing the hydrogeology at (A) accretionary margins, like SHR, and (B) non-accretionary, or erosional, margins. Solid black arrows represent the increase in fluid production with depth due to compaction and mineral dehydration. The blue arrows represent the relative magnitude and direction of flow, while the thick dashed line represents the décollement. (Figure from Kastner et al., 2014).

Quantifying fluid flow at seep sites is helpful in understanding the role of continental margin fluid flow in marine geochemical cycles. Quantification can also aid in the understanding of microbial and benthic population dynamics as these communities are sustained by both chemical transport by sub seafloor fluid advection and geochemical fluxes from the overlying water. (Suess 2014; Tryon et al., 2002). There are many seeps, however, where fluid is more seawater-like in composition due to and/or modified by in situ biogeochemical interactions which do not indicate transport from depth within the subduction zone (e.g. Tryon et al., 2002; Torres et al., 2002; Haeckel et al., 2004; Haeckel et al., 2007; Solomon et al., 2008; Vanneste et al., 2011). Considering

that seeps may play an important role in the marine carbon cycle and the long-term composition of seawater (e.g. Kastner et al., 2014), it is critical to constrain the magnitude of fluid flux from cold seeps.

At subduction zones, there may be several sources of fluid expelled at seafloor seeps (Figure 1). The two primary internal sources of fluid derived from the accretionary prism of a subduction zone and under-thrust oceanic crust are compaction and mineral dehydration. Compaction is the largest source, accounting for ~80% of fluid entering the subduction system that is then released from sediment pore spaces during the early stages of subduction (Kastner et al., 2014). Temperature and pressure changes within the under-thrust sediments causes clay minerals to dehydrate, typically transitioning from smectite to illite to opal-A-opal-C; dehydration of clays and other hydrous minerals in the igneous crust account for the second most important internal source of fluid during early subduction.

There are two main approaches to measuring fluid output at subduction zones: bottom-up and top-down approaches. The bottom-up approach estimates fluid flow rates from compaction and mineral dehydration along the deformation front by using porosity reduction, thermal regimes, rates of subduction and sediment consolidation behavior (Screaton et al., 2002, Saffer 2003; Saffer and Tobin, 2011). The top-down approach uses fluid emissions at the surface to determine fluid flow rates at seeps (e.g. Le Pichon et al., 1991;1993, Henry et al., 1996; Torres et al., 2002; Solomon et al., 2008; Vanneste et al., 2011;). An ongoing fundamental problem is that the top down measurements are substantially higher than what the bottom-up estimates.

These previous top-down estimates of fluid flux at seep sites are based on solute profiles obtained from sediment cores, heat flow, and temperature profiles. These represent instantaneous flow rates and the models are based on the assumption that fluid flow rates are in steady state

(Torres et al., 2002). Instantaneous measurements are likely not indicative of net flow at continental margin seeps, as long term studies with direct measurements have found that flow is highly variable with periods of upward flow and downward flow of fluid (Solomon et al., 2008; Torres et al., 2002; Tryon et al., 2002). In order to understand directional flow regimes in these areas, long-term quantification is crucial in addressing the balance of inputs and outputs. In this paper, I present the results of long-term (>1 year) direct fluid flow rate measurements at a seep site, Einstein's Grotto, at Southern Hydrate Ridge on the Cascadia margin.

3. BACKGROUND

3.1 Previous Studies

Bottom-up estimations of fluid flow range from ~0.3 cm/yr for margin-wide intergranular flow in Cascadia (Hyndman and Davis, 1992) and 0.5-4 cm/yr along fault zones at the Costa Rica subduction zone (Lauer and Saffer, 2012). These estimates are consistent with direction measurements along the decollement at the Costa Rica subduction zone where flow rates over a 2 year period ranged from 0.5-2 cm/yr (Solomon et al., 2009). Estimates similar to these are common worldwide when using the bottom-up geophysical methods. To corroborate these estimates, top-down fluid flow measurements have been taken across continental margins worldwide.

The first focused fluid flux surveys started in the late 1980s – early 1990s at the Barbados margin, the Cascadia margin, and the Nankai margin (e.g. Carson et al., 1990; Le Pichon et al., 1991). These surveys estimated fluid flow rates based on the curvature of the solute profiles and thermal profiles at seeps (Carson et al., 1990); the measurements were instantaneous as the curvature of solute and thermal profiles can only provide a short snapshot of what the fluid flux was at that moment in time. Short-term deployments of benthic flux chambers were also used to measure fluid flow rates, however, measurements were made on the timescale of up to 300

minutes, or 5 hours (Carson et al., 1990). Fluid flow rates out of the sediment into the water column were calculated to be 1-150 m/yr (Le Pichon et al., 1990; 1992; Carson et al, 1990; Davis et al., 1990; Foucher et al., 1990).

In Cascadia, more in-depth measurements of flow started in the early 2000s. A 1998-99 study of Hydrate Ridge used the curvature in the solute profiles which calculate flow less than 10 cm/yr from shallow cores taken from clam beds and 10-250 cm/yr of flow from cores taken from regions of bacterial mats (Torres et al., 2002). Benthic flux meters were developed to extend study times beyond instantaneous measurements as well as complement pore water profiles and to provide information on the temporal variability of fluid flow rates in marine sediments – one of these meters is a chemical and aqueous transport (CAT) meter. An array of CAT meters were deployed during the same field program as Torres et al., 2002 (Tryon et al., 2002). CAT meters do not penetrate the seafloor, but rather trap a volume of water proximal to the seafloor and measure fluid and chemical fluxes between the seafloor and the above water column. The CAT meters were deployed for ~1 month, and showed high variability in flow rates at SHR, ~10-1000 cm/yr. There were varying periods of upward flow and downward flow, and flow oscillated over timescales of days to weeks (Tryon et al., 2002).

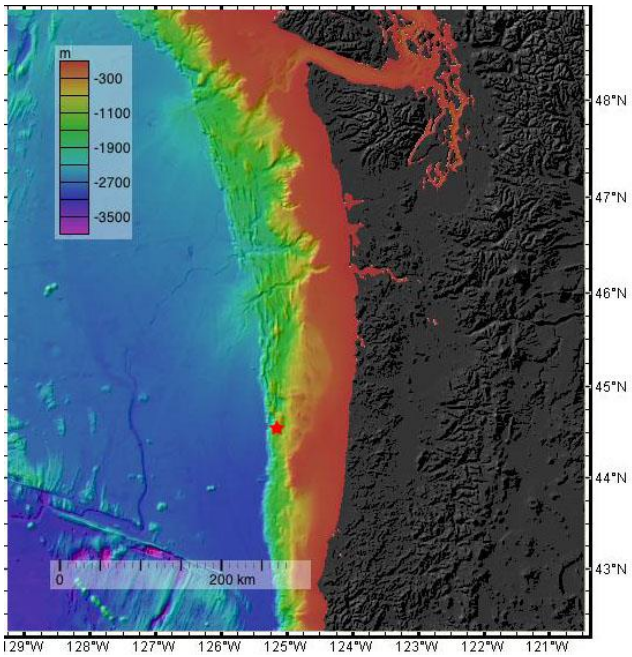

Figure 2. Bathymetry data along the Cascadia margin. Hydrate Ridge's location is marked by the red star.

3.2 Site Characteristics

The Cascadia subduction zone is a region in the northeastern Pacific, where the oceanic Juan de Fuca plate subducts beneath

the continental North American plate. Hydrate Ridge is located offshore Oregon on the second anticlinal ridge east of the deformation front of the Cascadia subduction zone (Haeckel et al., 2004). Hydrate Ridge has two active seep areas, Northern Hydrate Ridge (NHR) at a depth of ~600 m, and Southern Hydrate Ridge (SHR) at a depth of ~800 m (Tryon et al., 2001). It has also been the focus site of many studies (e.g. Torres et al., 2002; Tryon et al., 2002; Haeckel et al., 2004; Torres et al., 2004, etc.) as well as two Ocean Drilling Program coring cruises (Leg 146 NHR, Leg 204 SHR). Recently, Hydrate Ridge has become a fully instrumented location as part of the Ocean Observatories Initiative's Cabled Array.

Previous research focused on gas hydrate dynamics more than the hydrology, however, many factors about SHR are now constrained, such as subsurface geology and gas migration patterns. Comprehensive models of gas and fluids indicate that they flow along a highly conductive sand horizon, Horizon A, where the over-pressured gas, trapped beneath the regional methane hydrate stability zone (RHSZ) migrates through fractures and is expelled at the seafloor (Bangs et al., 2011). The substantial amount of information known about SHR is why it is the chosen study site to investigate the discrepancies between the bottom-up geophysical fluid transport models and the top-down geochemical measurements.

4. METHODS

4.1 The Mosquito Flow Meter

The Mosquito can continuously record fluid flow rates and fluid composition over a period of years. The Mosquito frame has a release plate with an array of titanium (Ti) needles which can be triggered during deployment, pushing the needles into the sediment. During these deployments, the Mosquito has 9 Ti needles, eight of which are joined to a long coil of Teflon tubing that is connected to an osmotic pump (Figure 3). The osmotic pumps, called OsmoSamplers (e.g.

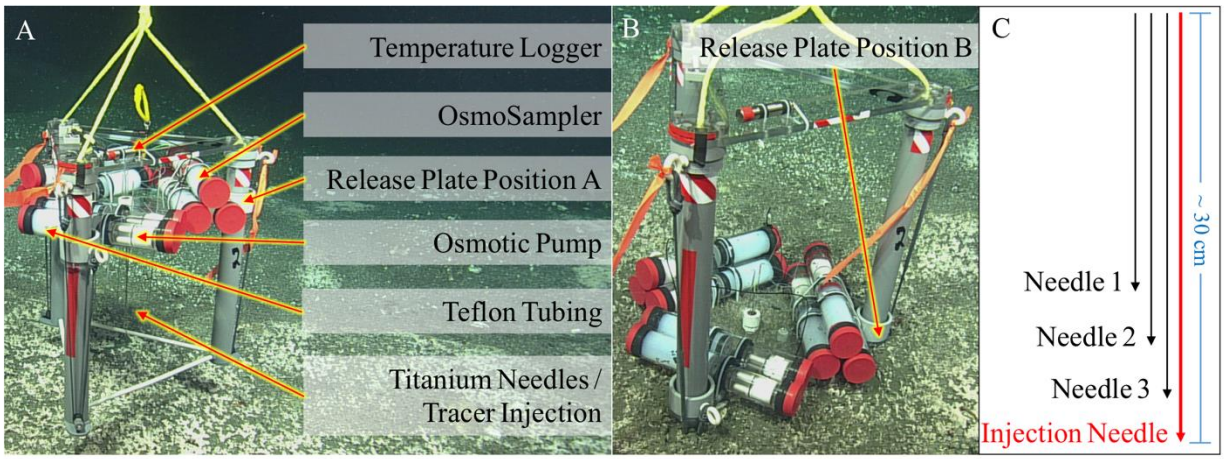

Figure 3. **(**A**)** Mosquito before deployment. (B) Mosquito, post deployment, at Einstein's grotto on top of bacterial mats that surround the methane seep site. (C) Vertical needle schematic in relation to the tracer injection needle. Each needle collects fluid in a respective coil, i.e. Needle 1 collects fluid in Coil 1.

Jannasch et al., 2004) draw pore fluid through the Ti needles into the Teflon coils where they are stored until instrument recovery. The osmotic pump relies only on the osmotic gradient within the pump and requires no external power, which allows it to be deployed for long time scales – typical deployments are 1-5 years. These 8 sampling needles are positioned at a known height and distance away from a tracer injection needle. There are 4 needles that sample fluid in the vertical direction, and 4 needles which sample in the lateral direction. After the needles are inserted into the sediment, 0.6mL of fluorescein, a nonreactive tracer, is injected into the seafloor via the tracer injection needle. A time-series of the tracer concentrations and fluid composition are collected in the Teflon tubing through the needles powered by the osmotic pump. The onset of the tracer in the time series and the shape of the concentration time series are then used to model the flow rates.

4.2 Mosquito Subsampling

Two Mosquitos used in this study, FLBON-M1 and MOS-2, were deployed on 17 July 2013 on the Ocean Observatories Initiative (OOI) Visions'13 cruise, and recovered on 2 September 2014 on OOI's Visions'14 cruise for a total deployment of ~411 days. Another deployment of a Mosquito, FLOBN-M2, was on 2 September 2014 on OOI's Visions'14 cruise

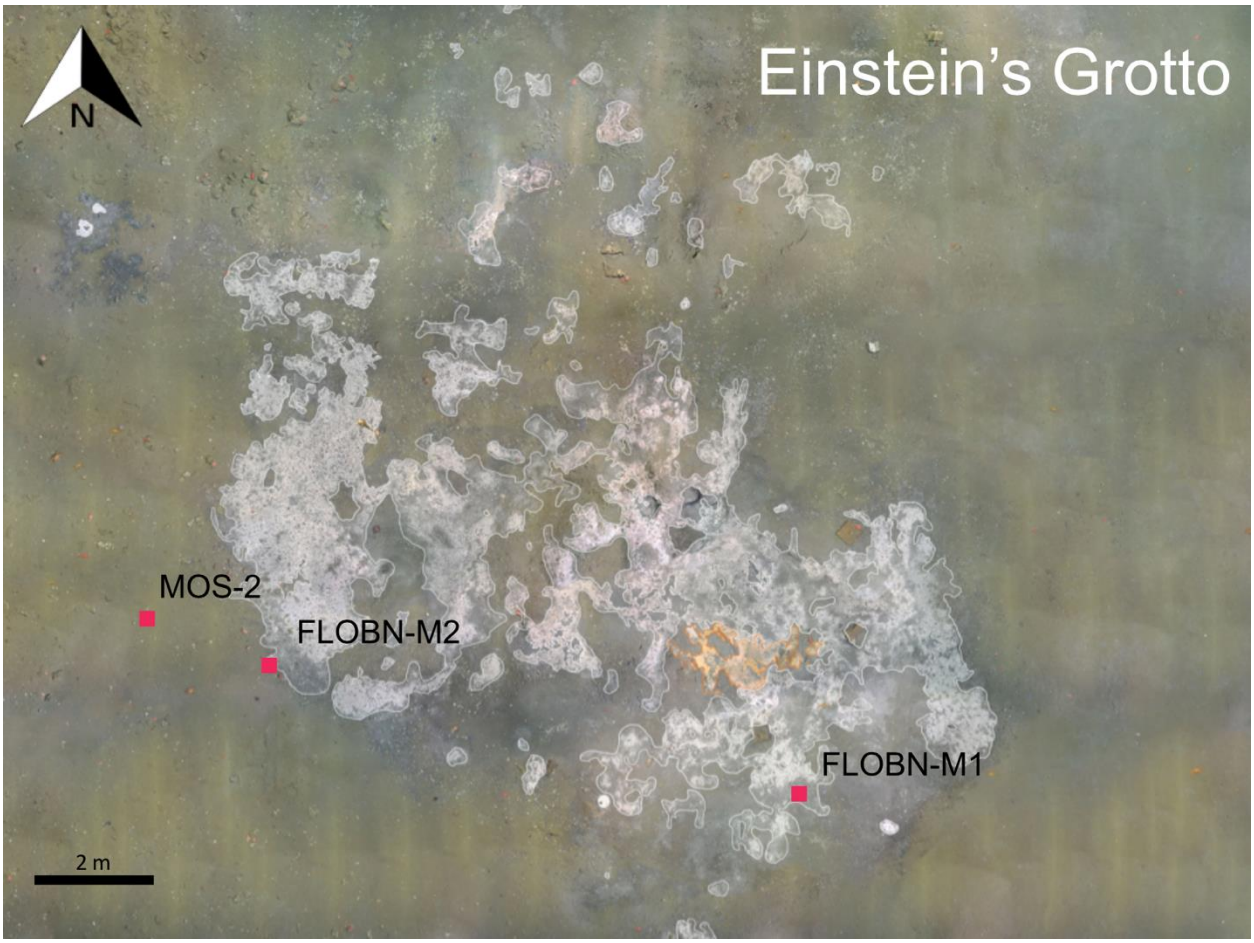

Figure 4. Location of each Mosquito at Einstein's Grotto on Southern Hydrate Ridge. This mosaic of Einstein's Grotto is from 2011. Although the spatial extent of the bacterial mat area is temporally variable, this general region has remained relatively consistent. FLOBN-M1 and MOS-2 were recovered in the summer of 2014, and FLOBN-M2 was recovered the summer of 2015. Each was deployed for about one year.

and recovered on 15 July 2015 on OOI's Visions'15 cruise for a total deployment of ~316 days (Figure 4). The *R/V Thomas G. Thompson* and the Canadian Scientific Submersible Facility's remotely operated vehicle (ROV) *ROPOS* were used for all deployment and recovery operations.

The coils of Teflon tubing containing the pore water samples were subsampled shipboard at ~4 day resolution. Onshore, a Cary Eclipse fluorescence spectrophotometer was used to analyze the Mosquito subsamples for fluorescein tracer concentrations to create a tracer concentration time series for each viable vertical coil. The standards used to calibrate the instrument ranged between 10^{-6} – 10^{-3} g/L fluorescein, and the precision of analyses were within 2.1% as determined from

repeat measurements of a 10^{-5} g/L fluorescein standard. Accuracy of measurements was 5.6% based on measurements of test standards of known concentrations.

4.3 Model Analysis

The tracer concentration time-series is used to quantify fluid flow rates using a 1-D advection-diffusion model based on the advection-diffusion equation (1)

$$\frac{\partial C}{\partial t} = D_s \frac{\partial^2 C}{\partial x^2} - v \frac{\partial C}{\partial x} \quad (1)$$

where D_s is the diffusivity coefficient, C is the concentration, t is time, x is distance, and v is flow rate. The analytical solution to equation 1, and what is used in the model is

$$C = \frac{C_0 V_0}{4\pi D_s t * 24 * 3600} * \exp\left(\frac{-(x - \sum vt\prime)^2}{(4 D_s t * 24 * 3600)}\right) \quad (2)$$

where C is the concentration, C_0 is the original concentration of fluorescein, V_0 is the original volume of fluorescein, D_s is the diffusivity coefficient, x is the distance from the injection needle, t is the time interval of deployment, v is the advection velocity, and t' is the time over which a specific advection velocity occurred. Equation 2 calculated fluorescein concentrations assuming isotropic sediment and a point source tracer injection (Baetsle 1969), both reasonable assumptions since all measurements are made between 15 and 50 cm below seafloor (cmbsf). This analysis is performed for each viable vertical needle for all three Mosquitos. The non-steady state model is unique as it can change the flow rate over different periods of time in the concentration time series. The model's parameters are needle depth relative to the tracer injection point, the concentration and volume of tracer injected into the sediment, the diffusion coefficient of fluorescein in the sediment, as well as pore water velocity. In order to calculate the diffusion coefficient of fluorescein in the sediment, D_{sed}, the diffusion coefficient of fluorescein in seawater, D_{aq}, was calculated using the Wilke and Chang (1955) equation

$$D_{aq} = \frac{7.4*10^{-8}*T*\sqrt{2.6m_{sol}}}{\eta V'^{0.6}} \quad (3)$$

where T is temperature in Kelvin, m_{sol} is the molecular weight of the solvent, η is the dynamic viscosity of the solution at *in situ* temperature and salinity, and $V^{'}$ is the molar volume of the diffusing substance (Satterfield, 1970). Using the porosity data from cores taken at the Mosquito sites during recovery, the average porosity measurement, ϕ, was used to calculate tortuosity, θ^2.

$$\theta^2 = 1 - \log(\phi^2) \quad (4)$$

The D_{aq} and θ^2, were then used to calculate D_{sed} which was used in equation 1.

$$D_{sed} = \frac{D_{aq}}{\theta^2} \quad (5)$$

This model allowed me to vary the input of flow rates over a period of time through the concentration time series, thus creating modeled concentrations of fluorescein that would be a result of the inputted flow rates. Iterations of different flow rates were entered into the model so that ideally the modeled concentrations of fluorescein match the observed concentrations of fluorescein in the samples. The flow rates for the time series create a flow rate history for each of the vertical needles analyzed. By integrating the flow rate history over the course of the Mosquito deployment the net fluid flow direction and magnitude was determined.

5. RESULTS

The Mosquito tracer concentration time series are for each vertical coil for each of the three Mosquitos deployed, FLOBN-M1, MOS-2, and FLOBN-M2. FLOBN-M1 and MOS-2 were deployed between 2013-2014, and FLOBN-M2 was deployed in 2014-2015. The figures represent the tracer concentration measured as well as the modeled tracer concentration for each Mosquito. In order to match the modelled concentrations of fluorescein to the observed concentrations of fluorescein, varying flow rates over varying periods of time were entered into the 1-D advection-diffusion model. The arrival of tracer and its concentration in the time series is a function of

distance away from the tracer injection needle and the fluid flow rate (Figure 3). Because Coil 3 has the closest needle to the tracer injection source, tracer arrives first and in high concentrations and its flow rate history is only accurate close to the deployment period. Modeled fluorescein concentrations from Coil 3 have subsequently been excluded as Coils 1 and 2 can provide a clearer flow rate history over the study period. The arrival of fluorescein at Coil 2 is slightly delayed, and the arrival of fluorescein at Coil 1 is even more delayed.

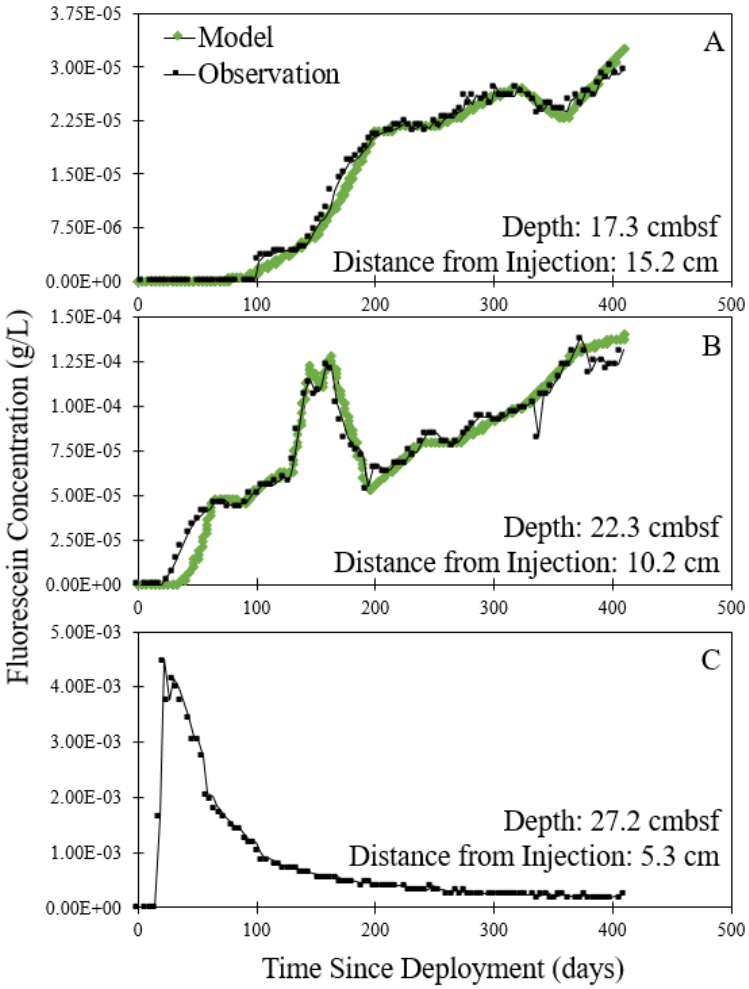

Figure 5. FLOBN-M1 modeled tracer concentration and observed concentration versus time deployed for Coil 1 (A), and Coil 2 (B), and the observed fluorescein concentration for Coil 3 (C). Injection needle depth is 32.5 cmbsf.

5.1 FLOBN-M1

Concentrations of fluorescein across FLOBN-M1 vary by up to three orders of magnitude with Coil 3 experiencing the highest concentrations of fluorescein and Coil 1 experiencing the lowest as expected (Figure 5). Around day 100, there was an intense increase in tracer concentrations in Coil 2, and the onset of this upwards flow is also registered in Coil 1 as the start of the time series for Coil 1.

5.2 MOS-2

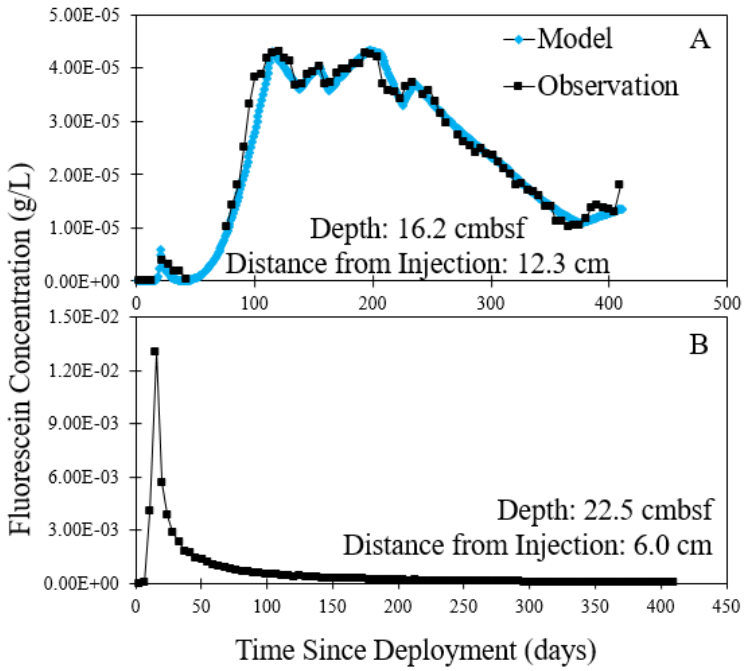

Figure 6. MOS-2 modeled tracer concentration and observed concentration versus time deployed for Coil 2(A), and the observed fluorescein concentration for Coil 3 (B). No fluorescein detected in Coil 1. Injection needle depth is 28.5 cmbsf.

Only two time series from MOS-2, are presented as no tracer concentration was recorded in Coil 1, the coil furthest away from the tracer injection source (Figure 6). Coil 3 in MOS-2 behaves as expected with a profile indicating that fluorescein, once injected, passed Coil 3 after around 75 days. The time series for Coil 2 picks up around day 75 and the oscillations of changing flow direction can easily be seen. The flow direction, as seen in Coil 2's time series, changes about every week and a half for a 125-day period, and then the direction of flow is steady downward flow. The end of the time series in Coil 2 suggests a period of upwards flow during the recovery of MOS-2.

5.3 FLOBN-M2

FLOBN-M2 yielded similar profiles to FLOBN-M1, however there was a continued source of tracer to the coil via advection or diffusion processes (Figure 7). There is a large spike in tracer concentration around day 10 in Coil 3, which corresponds to the arrival of tracer at Coil 2 about 5-10 days later. Coil 3 behaves differently in FLOBN-M2 than the other two Mosquitos as it spikes in concentration but does not indicate an immediate passing of the tracer. It appears that fluorescein was located near this Coil 3 longer than in the other Mosquitos' Coil 3. There appear to be

oscillations in the data near the middle to end of the record, seen in Coils 1 and 2, that are on a time scale of about 100 days.

5.4 Flow Rate Histories

The varying flow rates over the course of the deployment period are represented flow rate histories for Coil 1 and Coil 2 for each of the three Mosquitos (Figure 8). Only flow rate histories from Coils 1 and 2 are presented because those coils are more representative of the entire time series as they record the tracer's movement through the sediment column for the majority of the time the Mosquito was deployed. Coil 1, especially, demonstrates the movement of fluorescein and fluid late in the time series. It is evident that the flow rates represented in the flow rate histories are exceptionally variable and change in magnitude and direction over the course of many days to weeks.

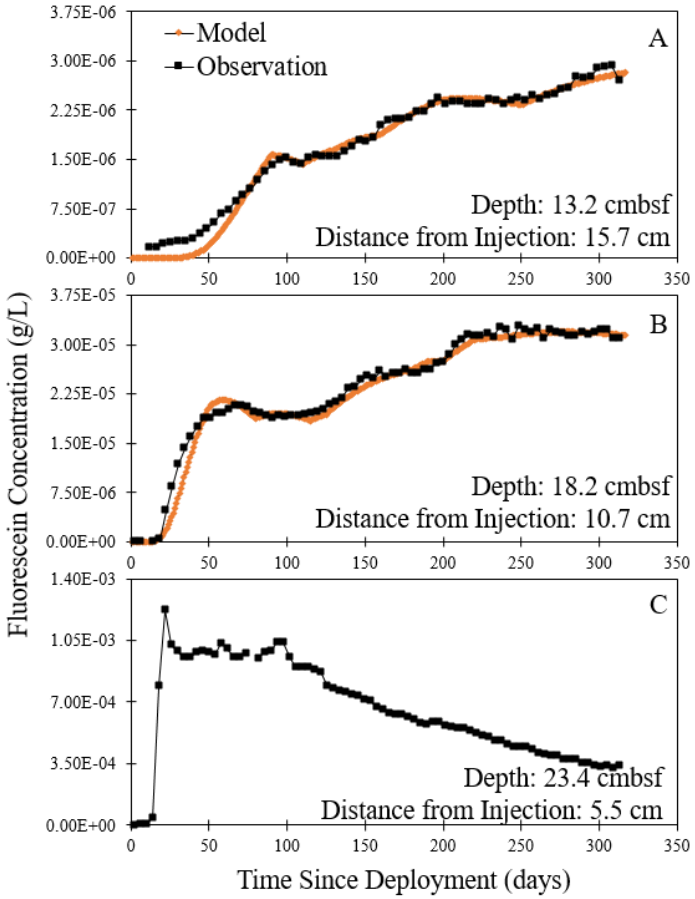

Figure 7. FLOBN-M2 modeled tracer concentration and observed concentration versus time deployed for Coil 1 (A), and Coil 2 (B), and the observed fluorescein concentration for Coil 3 (C). Injection needle depth is 28.9 cmbsf.

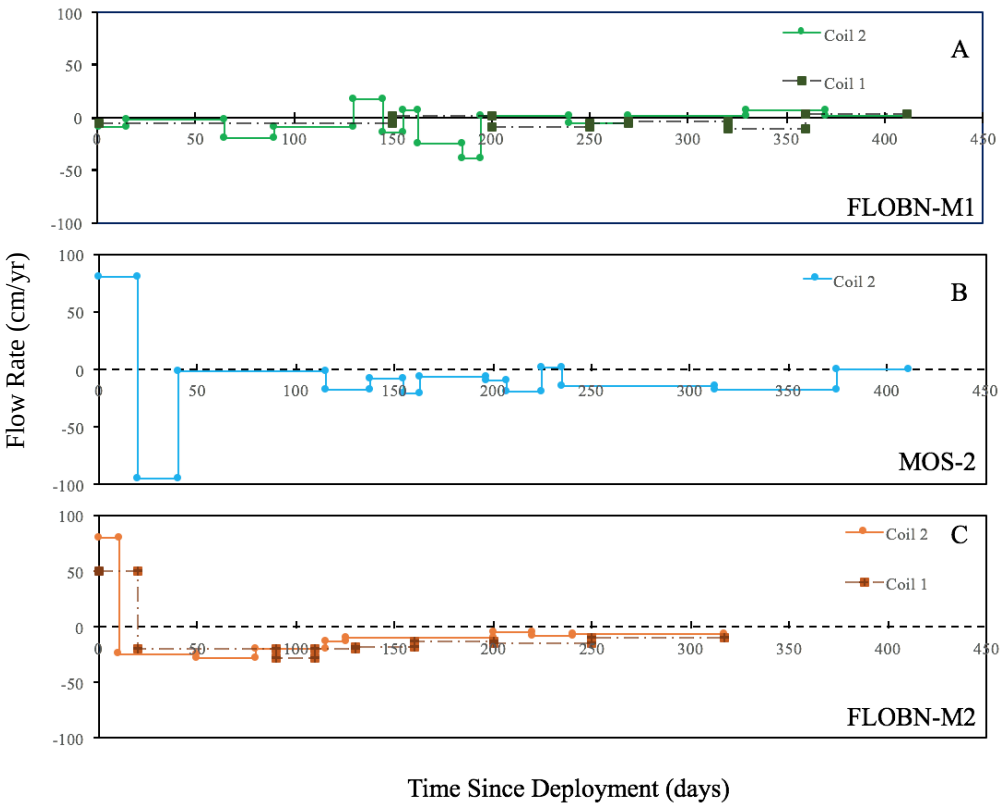

Figure 8. Flow rate histories from each Mosquito: FLOBN-M1. (A), MOS-2 (B), and FLOBN-M2 (C).

5.5 Net Flow Rates

The integration of these flow rates from the flow rate histories over the total time the Mosquitos were deployed is described as the net flow and the magnitude of the net flow for each Mosquito (Table 1).

Table 1. Net flow rates calculated from a reaction-transport model for Coils 1 and 2. The integrated flow is an average of the net flow from each coil. Negative values indicate downward flow.

	FLOBN-M1 (cm/yr)	MOS-2 (cm/yr)	FLOBN-M2 (cm/yr)
Coil 1	-20.8	-	-60.0
Coil 2	-28.9	-67.8	-54.1
Net Average Flow Rate	-24.9 ± 1	-67.8 ± 4	-57.1 ± 3

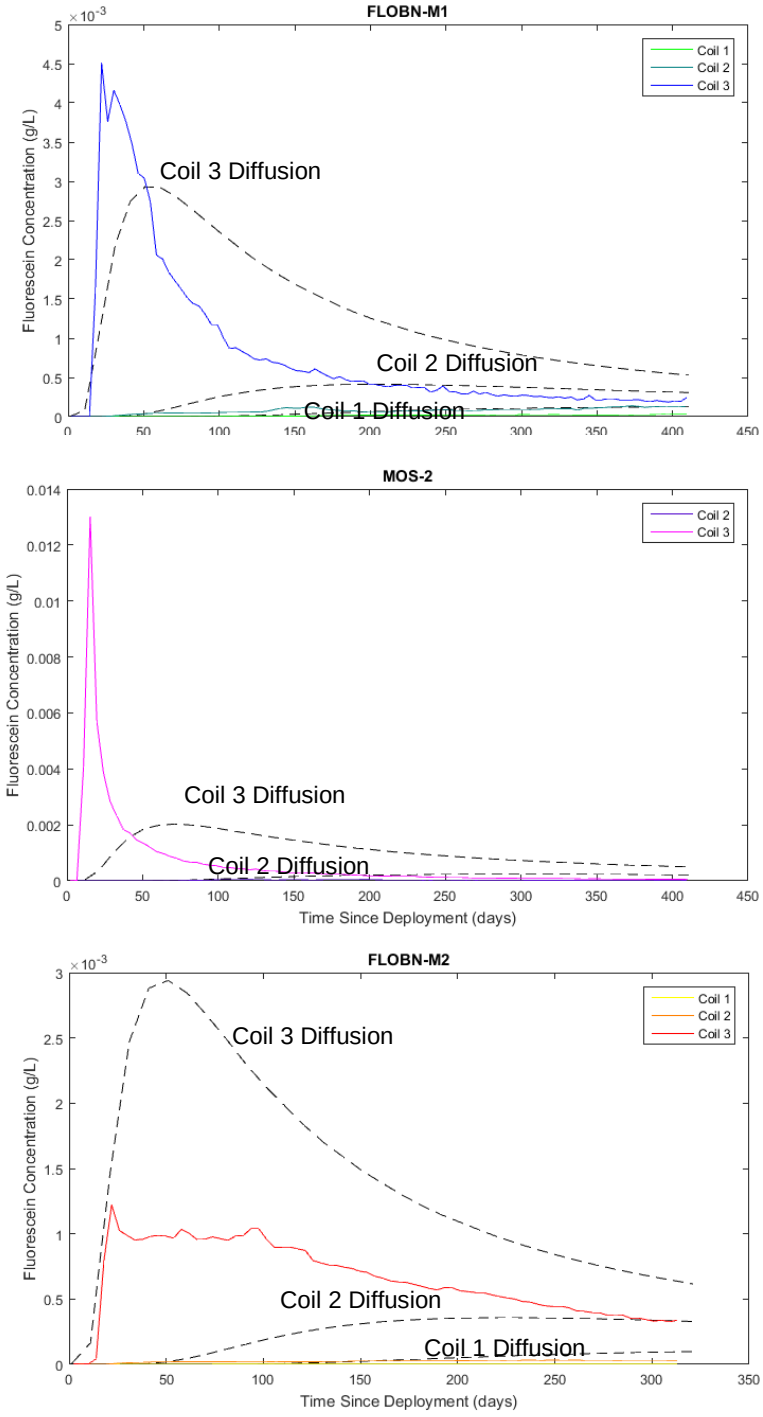

Figure 9. FLOBN-M1, MOS-2, and FLOBN-M2 observed concentrations plotted against diffusion curves for each coil's depth.

Figure 9 is a visual representation of the net downward flow across all Mosquitos. Despite a short period of tracer concentrations above the diffusion curve, which indicates upward flow, the majority of the tracer concentrations are well below the diffusion curve, indicating primarily downward flow. There must be net downward flow in order for the tracer concentrations to fall below the diffusion curve.

Although deployed during separate periods, MOS-2 and FLOBN-M2 were deployed in close proximity, ~2 m apart from each other. Interestingly these two Mosquitos show a similar integrated flow rate with -67.82 ± 4 cm/yr between 2013-2014 and 57.07 ± 3 cm/yr between 2014-2015.

6. DISCUSSION

6.1 Summary

Based on figure 9, it is evident that there is a general trend of downward flow at the three Mosquito sites at SHR. Seawater pore fluid composition in the upper sediment column has been previously observed confirming the notion that there is downward flow of seawater into the sediment (Torres et al., 2004). The continuous aqueous transport (CAT) samplers recorded periods of downward flow and noted it was more prevalent than previously thought (Tryon et al., 2001, Tryon et al., 2002). Knowing that downward flow is more common than thought could explain the widespread observed seawater composition of pore water in sediment cores collected at seep sites (e.g. Torre et al., 2002; Solomon et al., 2008). In the Gulf of Mexico, Mosquito deployments over 15 months indicated that there was chronic downward flow at gas seep sites (Solomon et al., 2008). The new Mosquito flow rate record at SHR indicates chronic downward flow over 2 years in bacterial mats.

6.2 Mechanisms driving downward flow

Bubbles in the marine sediment column are due to methane transport from depth along permeable fractures and sand horizons – as pressure decreases along the permeable pathways, gas bubbles form. Clay-like sediment, such as that in the upper sediment column at SHR, reacts to bubbles as a plastic solid that fractures elastically (Boudreau et al., 2005). Thus as bubbles form and grow, they fracture the surrounding sediment as a result of buoyancy. The fracturing and discharge of gas bubbles through a conduit decreases pressures to below lithostatic which causes downward fluid flow to recover hydrostatic pressure (Tryon et al., 2002). Downward flow must then occur at SHR due to episodic release of gas from sub-surface reservoirs.

Gas dissolution can occur while bubbles are rising throughout the sediment column. This occurs when the methane, the primary gas in these bubbles, is not in saturation in the surrounding

sediment column, thus the gas diffuses out of the bubble creating a volume decrease. The volume decrease causes seawater then travels down into the sediment to fill. When considering the volume change associated with gas dissolution, Haeckel et al., calculated a fluid flow rate of -51.4 cm/yr (2004).

6.3 Mechanisms driving upward flow

Although there is a general trend of downward flow, there are periods of upward flow observed in all Mosquito tracer concentration time series. One process responsible for driving upward flow is gas hydrate formation. Gas hydrate formation, at SHR and other gas seeps, can expel fluids out of the sediment due to the increase in volume of hydrate. This pore space reduction, as gas hydrate forms, pushes the fluids out of the pore space and is directed upward (e.g. Haeckel et al., 2004). Water can also be expelled from the sediment column as bubbles displace the confining fluid when the sediment is fractured and bubble flow is induced due to the high conductivity of that fracture.

6.4 Persistence of bacterial mats with chronic downward flow

Tryon et al., 2002 suggested the benthic biota at seep sites reflects different flow regimes, i.e. bacterial mats are indicators of upward flow and vesicomyid clams are indicators of downward flow. Tryon et al. (2002) also suggested that a circulation cell of seawater exists between regions of bacterial mats and regions of vesicomyid clams. This current Mosquito study at SHR has major implications for benthic ecology at seep sites as chronic downward flow was observed in regions of bacterial mats.

One possible reason why bacterial mats persist in apparent downward flow regimes is gas dissolution providing methane. Gas is able to rise above the regional hydrate stability zone (RHSZ) without being formed into solid gas hydrate when there is oversaturation of gas below the RHSZ

and an over pressurization of gas below a gas hydrate cap which thus creates a fracture in the hydrate cap (Liu and Flemings, 2007). Gas can then bypass and it is able to rise in the sediment column; as the gas rises, it undergoes dissolution due to the low concentrations of that gas in the above layers of the RHSZ. We propose that this process provides methane to allow the anaerobic oxidation of methane (AOM) to occur at shallower depths, and thus providing the hydrogen sulfide needed to support the *Beggiatoa* bacterial mats at shallower depths bypassing the need for advection via upward fluid flow. Another possible reason why these bacterial mats persist during periods of downward flow is that they take advantage of short bursts of upward flow that occur at time scales much smaller than the ~4 day resolution of the Mosquito subsamples.

Further research is needed to constrain the dynamics of bacterial mats at cold seep sites. Over the course of the deployment to the recovery of the Mosquitos there was a change in the extent and condition of the bacterial mats. At the Mosquito recovery sites, the bacterial mat had receded and was noticeably grayer than the lush white mat around it between the 2013 deployment and the 2014 recovery. It would be beneficial to have a visual record for the bacterial mat over the course of the Mosquito deployment. A digital still camera could be connected to OOI's SHR site and record the bacterial mat creating a temporal and spatial record of the bacterial mat that could be correlated with periods of upwards or downwards flow from the Mosquito time series and flow rate histories. Chemically, high resolution H_2S and CH_4 data are needed to see if there is a secondary zone of AOM above the regional sulfur methane transition zone to correlate bacterial mat persistence with gas dissolution.

6.5 Imbalance of bottom up and top down measurements

A possible reason why this discrepancy exists is because bottom-up measurements can only account for the fluid produced at depth rather, top-down measurements observe mixing between

the small source of fluid output and circulating seawater at the interface of the sediment and bottom water. Bottom-up estimates are on the order of mm/yr of fluid flow versus top-down measurements of 100's of cm/yr fluid flow at the surface, thus this has very important implications on geochemical cycles. The mixing between the small amount of deep sourced fluids and seawater could indicate overestimates of element fluxes like Li, B, etc. However, the seawater residence time in the sediment column is needed in order to determine just how important the impacts that seawater circulation has on biogeochemical cycles.

7. CONCLUSION

Observed chronic downward flow of seawater at seep sites is a result of shallow seawater circulation driven by hydrate and gas dynamics. This is a surprising notion, as chronic downward flow was observed in bacterial mats, which were thought to be indicators of regions of upward flow. This goes against conventional thinking and future work focusing on the mechanism for sustaining the benthic seep communities with chronic downward flow is needed.

References

Baestle, L. H. 1969. Migration of radionuclides in porous media, 707-730. *In* Prog. Nucl. Energ XII: Health Physics. Duhamel, A. M. F. (ed.).

Bangs, N. L. B., M. J. Hornbach, C. Berndt. 2011. The mechanics of intermittent methane venting at South Hydrate Ridge inferred from 4D seismic surveying. Earth Plant. Sci. Lett. 310: 105-112.

Boetius, A., E. Suess .2004. Hydrate Ridge: a natural laboratory for the study of microbial life fueled by methane from near-surface gas hydrates. Chem. Geol. 205: 291-310.

Carson, B., E. Suess, J. C. Strasser. 1990. Fluid Flow and Mass Determinations at Vent Sites on the Cascadia Margin Accretionary Prism. J. Geophys. Res. 95: 8891-8897.

Haeckel, M., E. Suess, K. Wallmann, D. Rickert. 2004. Rising methane gas bubbles form massive hydrate layers at the seafloor. Geochim. Cosmochim. Ac. 68: 4335-4345.

Haeckel, M., B. P. Boudreau, K. Wallmann. 2007. Bubble-induced porewater mixing: a 3-D model for deep porewater irrigation. Geochim. Cosmochim. Ac. 71: 5135-5154.

Henry, P., X. Le Pichon, S. Lallemant, S. Lance, J. B. Martin, J. Foucher, A. Fiala-Medoni, F. Rostek, N. Guilhaumous, V. Pranal, M. Castrec. 1996. Fluid flow in and around a mud volcano field seaward of the Barbados accretionary wedge: Results from Manon cruise. J. Geophys. Res. 101:20,297-20,323.

Hyndman, R. D., E. E. Davis. 1992. A mechanism for the formation of methane hydrate and sea-floor bottom-simulating reflectors by vertical fluid expulsion. J. Geophys. Res. 97: 7025-704.

Kastner, M., E. A. Solomon, R. N. Harris, M. E. Torres. 2014. Fluid Origins, Thermal Regimes, and Fluid and Solute Fluxes in the Forearc of Subduction Zones, 671-722. *In* Developments in Marine Geology, Volume 7. Elsevier. Stein, R., D. K. Blackman, F. Inagaki, H. Larsen (ed.).

Lauer, R. M., D. M. Saffer. 2012. Fluid budgets of subduction zone forearcs: The contribution of splay faults. Geophys. Res. Lett. 39. doi: 10.1029/2012GL052182.

Le Pichon, X., P. Henry, The Kaiko-Nankai Scientific Crew. 1991. Water budgets in accretionary wedges: a comparison. Phil. Trans. R. Soc. Lond. A. 335: 315-330.

Le Pichon, X., P. Henry, S. Lallemant. 1993. Accretion and erosion in subduction zones: the role of fluids. Annu. Rev. Earth Planet. Sci. 21: 307-331.

Liu, X. L., P. B. Flemings. 2007. Dynamic multiphase flow model of hydrate formation in marine sediments. J. Geophys. Res. – Sol. Ea. 112. doi: 10.1029/2005JB004227.

Moore, G., D. Saffer, M. Studer, P. Costa Pisani. 2011. Structural restoration of thrusts at the toe of the Nankai Trough accretionary prism off Shikoku Island, Japan: Implications for dewatering processes. Geochem. Geophys. Geosyst. 12. doi: 10.1029/2010GC003453.

Saffer, D. M., E. J. Screaton. 2003. Fluid flow at the toe of convergent margins: interpretation of sharp pore-water geochemical gradients. Earth Planet. Sci. 213: 261-270.

Saffer, D. M., H. J. Tobin. 2011. Hydrogeology and Mechanics of Subduction Zone Forearcs: Fluid Flow and Pore Pressure. Annu. Rev. Earth Planet. Sci. 39:157-186.

Satterfield. 1970. Mass Transfer in Heterogeneous Catalysis. MIT Press, Cambridge Mass., 267pp.

Screaton, E. J., D. Saffer, P. Henry, S. Hunze. 2002. Porosity loss within the underthrust sediments of the Nankai accretionary complex: Implications for overpressurese. Geol. Soc. Am. 30:19-22.

Suess, E. 2014. Marine cold seeps and their manifestations: geological control, biogeochemical criteria and environmental conditions. Int. J. Earth. Sci. 103:1889-1916.

Solomon, E. A., M. Kastner, H. Jannasch, G. Robertson, Y. Weinstein. 2008. Dynamic fluid flow and chemical fluxes associated with a seafloor gas hydrate deposit on the northern Gulf of Mexico slope. Earth Planet. Sc. Lett. 270:95-105.

Solomon, E. A., M. Kastner, C. G. Wheat, H. Jannasch, G. Robertson, E. E. Davis, J. D. Morris. 2009. Long-term hydrgeochemical records in the oceanic basement and forearc prism at the Costa Rica subduction zone. Earth Planet. Sci. Lett. 282: 240-251.

Torres, M. E., J. McManus, D. E. Hammond, M. A. de Angelis, K. U. Heeschen, S. L. Colbert, M. D. Tryon, K. M. Brown, E. Suess. 2002. Fluid and chemical fluxes in and out of sediments hosting methane hydrate deposits on Hydrate Ridge, OR, I: Hydrological provinces. Earth Planet. Sc. Lett. 201: 525-540.

Tryon, M. D., K. M. Brown, M. E. Torres. 2002. Fluid and chemical fluxes in and out of sediments hosting methane hydrate deposits on Hydrate Ridge, OR, I: Hydrological processes. Earth Planet. Sc. Lett. 201: 541-557.

Vanneste, H., B. A. Kelly-Gerreyn. D. P. Connelly, R. H. James, M. Haeckel, R. Fisher, K. Heeschen, R. A. Mills. 2011. Spatial variation in fluid flow and geochemical fluxes across the sediment-seawater interface at the Carlos Ribeiro mud volcano (Gulf of Cadiz). Geochim. Cosmochim. Ac. 75: 1124-1144.

Wilke, C. R., P. Chang. 1955. Correlation of diffusion coefficients in dilute solutions. AICHE. 1: 264-270.